Electronic Supplementary Material (ESI) for Chemical Communications.
This journal is © The Royal Society of Chemistry 2021

Electronic Supplementary Information

Efficient NIR electrochemiluminescent dyes based on ruthenium(II) complexes containing an N-heterocyclic carbene ligand

Yu-Yang Zhou,*[a,b] Yang-Ming Ding,[b] Wei Zhao,[a] Jian-Hua Dong,[b] Liang-Zhi Li,[b] Hong-Yuan Chen,[a] Jing-Juan Xu*[a,c]

[a.] State Key Laboratory of Analytical Chemistry for Life Science, School of Chemistry and Chemical Engineering, Nanjing University, Nanjing 210023, China. E-mail: xujj@nju.edu.cn; zhouyuyang@mail.usts.du.cn. Tel./Fax: +86-25-89687294.

[b.] School of Chemistry and Life Sciences, Suzhou University of Science and Technology, Suzhou 215009, China. E-mail: zhouyuyang@mail.usts.du.cn.

[c.] College of Chemistry and Molecular Engineering, Zhengzhou University, Zhengzhou 450001, China

1. Experimental Section

Chemicals. N,N-Dimethylformamide (DMF), ethanol and acetonitrile (AR grade) are from Jiangsu Qiangsheng Functional Chemistry Co., Ltd. Anhydrous acetonitrile (extra dry) and tetra-n-butylammonium hexafluorophosphate ($TBAPF_6$) for electrochemical and ECL characterization are purchased from Energy Chemical Inc. (Shanghai, China) and J&K Chemical Ltd. 4,7-diphenyl-1,10-phenoline (DIP), 1H-benzo[d]imidazole, iodobenzene, 1-iodo-4-(trifluoromethyl)benzene, CuI, L-proline and dichloro(p-cymene)ruthenium(II)dimer $[Ru(p\text{-cymene})Cl_2]_2$ and other chemicals for synthesizing ruthenium(II) complexes in this work are all obtained from commercial suppliers and used as received without further purification.

Apparatus and Methods. ^{1}H-NMR and ^{13}C-NMR spectra were all acquired from VARIAN 400 MHz magnetic resonance spectrophotometer. Mass spectra were measured on a Varian ProStar LC240. UV-vis spectra and photoluminescent spectra were recorded on a UV-vis spectrophotometer (TU-1950, Beijing Purkinje General Instrument Co., Ltd, Beijing, China) and an Edinburgh FLS920 type steady-state/ transient spectrometer, respectively. FT-IR data were collected on PerkinElmer Spectrum Two FT-IR spectrometer. The melting points (M.p.) were recorded on optical micro melting point instrument (SGW$^{@}$, X-4A, shenguang, Shangshai). The CV and ECL photocurrent signals were collected out on CHI650E (Chenhua Instruments Ltd., Shanghai, China) and MPI-EII ECL detector (Xi'an Remax Electronics, China) equipped with a photomultiplier tube (Model: R9880U-20, Hamamatsu, Japan, spectral response range: 230-920 nm), respectively. The ECL spectra of these RuNHC complexes have also been recorded under potential stepping mode by combining the electrochemical workstation (CHI650E) and Edinburgh FLS920 spectrometer (excitation light is off).

Electrochemical experiments were performed using a three-electrode setup with glassy carbon as working electrode (diameter is 3 mm, sealed in PEEK), a platinum rod as auxiliary electrode and a platinum wire as quasi-reference electrode. The working electrode was polished after each experiment with 0.3 μm alumina (Gaussian Union)

for several minutes, sonicated in water and in ethanol for 5 min each, and dried with a warm air flow. All the electrochemical potential (E) was initially calibrated against the internal reference of Fc/Fc^+ couple and the obtained potentials were all finally converted to E vs NHE (normal hydrogen electrode) through the redox potential of Fc/Fc^+ vs NHE (E=0.63 V) in this work.[1] The ECL efficiency (Φ_{ECL}) is calculated using the equation: $\Phi_{ECL}^{S} = \Phi_{ECL}^{R}(I_S/I_R)(Q_R/Q_S)$,[2] where Φ_{ECL}^{R} is the ECL efficiency of reference ($Ru(bpy)_3^{2+}$ is the reference in this work and the value is defined as 100%); I_S and I_R are the integrated ECL intensities of sample and reference, respectively; Q_S and Q_R are the charges (in Coulombs) passed for the sample and reference, respectively.

Theoretical calculations. All calculations were performed in the Gaussian09 packages. The density functional hybrid model B3LYP was used together with the 6-31G(d) basis set. The LANL2DZ basis set was finally employed for the metal atom and the 6-31G(d) basis set for the other atoms, including carbon, nitrogen, hydrogen, oxygen and fluorine. The energies of the frontier orbitals are obtained from single-point calculations incorporating a solvent model (CPCM, solvent is acetonitrile) on the optimized structures.

Synthesis and Characterizations. The NHC precursors of aryl-benzo[d]imidazolium salts ($L_{C\wedge C*}$) in this work synthesized through two main steps, including C-N Ullmann coupling reaction and quaternization reaction, while another three major steps would be employed for the final Ru-NHC complexes in this work. All the five steps are described in details as follows.

Step i: A mixture of 1H-benzo[d]imidazole (1 eq.), aryl halide (1.1 eq., iodobenzene for RuNHC-1, or 1-iodo-4-(trifluoromethyl)benzene for RuNHC-2), K_2CO_3 (2 eq.), catalytic amount of CuI (0.1 eq.) and L-proline (0.2 eq.) in DMF solution were heated to 90 ºC and stirred for 48 hours under argon atmosphere in dark conditions. After cooling to room temperature, the insoluble chemicals in the muddy solution was firstly filtrated and washed with dichloromethane for three times. The obtained solution was then added with saturated salt water and would be partitioned. The organic phase was washed with deionized water for three times and collected together. The combined organic solution was dried with anhydrous sodium sulfate and then concentrated in

vacuo. The residual oil was loaded on a silica gel column and eluted with the mixture solution of ethyl acetate and petroleum ether (v:v=1:5) to obtain the ideal intermediated product. For 1-phenyl-1H-benzo[d]imidazole (Yield: 72%). ^{1}H NMR (400 MHz, $CDCl_3$), δ (ppm): 8.10 (s, 1 H), 7.88 (m, 1 H), 7.56-7.45 (m, 6 H), 7.32 (m, 2 H); ^{13}C NMR (101 MHz, $CDCl_3$), δ (ppm): 143.95, 142.15, 136.23, 133.56, 129.92, 127.90, 123.91, 123.56, 122.66, 120.49, 110.34. For 1-(4-(trifluoromethyl)phenyl)-1H-benzo[d]imidazole (Yield:75%). ^{1}H NMR (400 MHz, DMSO-d_6), δ (ppm): 8.69 (s, 1 H), 8.00 (dd, J=8.4, 9.2 Hz, 4 H), 7.81 (d, J=7.2 Hz, 1 H), 7.73 (d, J=7.2 Hz, 1 H), 7.36 (m, 2 H); ^{13}C NMR (101 MHz, DMSO-d_6), δ (ppm): 144.02, 143.34, 139.44, 132.61, 127.31, 127.27, 124.06, 123.88, 122.94, 120.17, 110.85. For 1-(4-methoxyphenyl)-1H-benzo[d]imidazole (Yield: 37%). ^{1}H NMR (400 MHz, DMSO-d_6), δ (ppm): 8.45(s, 1 H), 7.76 (m, 1 H), 7.59-7.49 (m, 3 H), 7.30 (m, 2 H), 7.18-7.15 (m, 2 H), 3.85 (s, 3 H); ^{13}C NMR (101 MHz, DMSO-d_6), δ (ppm): 158.69, 143.60, 143.45, 133.60, 128.79, 125.44, 123.27, 122.20, 119.84, 115.13, 110.45, 55.54.

Step ii: A mixture of 1 eq. of N-aryl-benzo[d]imidazole and extra amount of methyl iodide (CH_3I) in THF solution are stirred for 12 hours at room temperature with protecting from light. The obtained quaternary ammonium salts would be precipitated from the solution. After filtration and washed with THF, the benzo[d]imidazolium salts as NHC precursors are obtained. For N-methyl-N'-phenyl-benzo[d]imidazolium iodized salt (White powder, Yield: 98%). M.p.: 196 ^{o}C. ^{1}H NMR (400 MHz, DMSO-d_6), δ (ppm): 10.14 (s, 1 H), 8.16 (d, J=8 Hz, 1 H), 7.79 (m, 8 H), 4.18 (s, 3 H); ^{13}C NMR (101 MHz, DMSO-d_6), δ (ppm): 143.16, 133.19, 131.90, 130.89, 130.49, 127.44, 126.94, 125.12, 113.98, 113.37, 33.53. For N-methyl-N-(4-(trifluoromethyl)phenyl)-benzo[d]imidazolium iodized salt (White powder, Yield: 97%). M.p.: 242 ^{o}C. ^{1}H NMR (400 MHz, DMSO-d_6), δ (ppm): 10.21 (s, 1 H), 8.18 (d, J=8.4 Hz, 3 H), 8.09 (d, J=8.4 Hz, 2 H), 7.93 (d, J=8.4 Hz, 1 H), 7.83-7.73 (m, 2 H), 4.19 (s, 3 H); ^{13}C NMR (101 MHz, DMSO-d_6), δ (ppm):143.51, 131.92, 130.65, 127.73, 127.69, 127.63, 127.12, 126.20, 114.08, 113.41, 33.63. N-methyl-N-(4-(4-methoxy)phenyl)-benzo[d]imidazolium iodized salt (White powder, Yield: 92%). M.p.: 252 ^{o}C. ^{1}H NMR (400 MHz, DMSO-d_6), δ (ppm): 10.07 (s, 1 H), 8.14 (d, J=8 Hz, 1 H), 7.75 (m, 5 H),

7.29 (d, J=9.2 Hz, 2 H), 4.17 (s, 3 H), 3.89 (s, 3 H); ^{13}C NMR (101 MHz, DMSO-d_6), δ (ppm): 160.45, 143.04, 131.73, 131.30, 127.26, 126.78, 126.71, 125.71, 115.42, 113.82, 113.23, 55.79.

Step iii: A mixture of 2 eq. imidazolium salt (abbreviated as $L_{C\hat{}C*}$), 1 eq. [Ru(p-cymene)Cl_2]$_2$ and 2 eq. Ag_2O in dichloromethane protecting from light are stirred for 48 hours at room temperature. The solvent was removed through rotary evaporation in vacuo and the crude product was carefully purified through silica column chromatography for three times (eluent solvent is CH_2Cl_2). For Chloro[1-(phenyl-κC^2)-3-methylbenzo[d]imidazolin-2-ylidene-κC^2][η^6-1-methyl-4-(1-methylethyl)benzene] ruthenium (II). Yield:19%, cyan solid. ^{1}H NMR (400 MHz, $CDCl_3$), δ (ppm): 8.20 (dd, J=7.2, 1.2 Hz, 1 H), 7.94 (m, 1 H), 7.65 (dd, J=8, 1.2 Hz, 1 H), 7.41 (m, 1 H), 7.32-7.29 (m, 2 H), 7.05 (m, 2 H), 5.70 (m, 2 H), 5.60 (d, J=6 Hz, 1 H), 5.49 (d, J=6 Hz, 1 H), 4.38 (s, 3 H), 2.18 (m, 1 H), 2.10 (s, 3 H), 0.87 (d, J=6.8 Hz, 3 H), 0.74 (d, J=6.8 Hz, 3 H). ^{13}C NMR (101 MHz, $CDCl_3$), δ (ppm): 204.75, 164.07, 148.22, 142.57, 137.48, 132.73, 125.19, 124.22, 123.63, 123.56, 113.74, 112.46, 110.86, 107.20, 101.31, 95.41, 92.56, 90.54, 86.68, 36.18, 32.27, 24.05, 23.04, 20.20. Chloro[1-(4-trifluoromethylphenyl-κC^2)-3-methylbenzo[d]imidazolin-2-ylidene-κC^2][η^6-1-methyl-4-(1-methylethyl)benzene] ruthenium (II). Yield:18%, cyan solid. ^{1}H NMR (400 MHz, $CDCl_3$), δ (ppm): 8.47 (s, 1 H), 7.94 (m, 1 H), 7.70 (d, J=8.4 Hz, 1 H), 7.43 (m, 1 H), 7.36 (m, 3 H), 5.73 (t, J=4.8 Hz, 2 H), 5.67 (d, J=6 Hz, 1 H), 5.53 (d, J=6 Hz, 1 H), 4.39 (s, 3 H), 2.15 (m, 1 H), 2.12 (s, 3 H), 0.87 (d, J=7.2 Hz, 3 H), 0.74 (d, J=6.8 Hz, 3 H). ^{13}C NMR (101 MHz, $CDCl_3$), δ (ppm): 204.20, 163.86, 137.35, 136.40, 131.44, 125.69, 123.48, 122.96, 120.24, 111.77, 111.28, 109.99, 107.00, 100.82, 94.53, 91.81, 89.71, 85.91, 35.12, 31.16, 22.88, 21.89, 19.04. Chloro[1-(4-methoxylphenyl-κC^2)-3-methylbenzo[d]imidazolin-2-ylidene-κC^2][η^6-1-methyl-4-(1-methylethyl)benzene] ruthenium (II). Yield: 21%, yellow solid. ^{1}H NMR (400 MHz, DMSO-d_6), δ (ppm): 8.12 (d, J=8.8 Hz, 1 H), 7.73 (m, 2 H), 7.65 (d, J=8.4 Hz, 1 H), 7.36 (m, 2 H), 6.53 (dd, J=8.4, 2.8 Hz, 1 H), 5.87-5.82 (dd, J=15.2, 5.6 Hz, 2 H), 5.76 (t, J=5.6 Hz, 2 H), 4.32 (s, 3 H), 3.81 (s, 3 H), 2.00 (m, 1 H), 1.98 (s, 3 H), 0.77 (d, J=7.2 Hz, 3 H), 0.62 (d, J=6.8 Hz, 3 H). ^{13}C NMR (101 MHz, $CDCl_3$), δ (ppm): 202.04, 164.92, 155.25, 141.22,

136.21, 131.32, 127.41, 122.96, 122.26, 112.44, 110.94, 109.71, 106.67, 106.01, 100.03, 94.07, 91.16, 89.45, 85.65, 55.49, 34.99, 31.11, 22.94, 21.88, 19.05.

Step iv&v: A mixture of the corresponding *p*-cymene ruthenium(II) intermediate (1 eq. and 4,7-diphenyl-1,10-phenoline(DIP, 2.1 eq.) were dissolved in ethanol solution and refluxed for 24 hours in argon atmosphere protecting from light. And then the reaction was cooled to room temperature and concentrated through rotary evaporation in vacuo. Subsequently, a large amount of saturated aqueous solution of NH_4PF_6 was added to the concentrated solution and stirred for 30 minutes. The precipitate was filtrated and the crude product was purified through silica column chromatography using the mixture eluent of ethyl acetate/dichloromethane (v:v=1:30~1:15). **RuNHC-1**, Yield: 90%, black solid. M.p: 265 ºC. IR (cm^{-1}): 1444 (w), 1380 (w), 1316 (w), 1205 (w), 1076 (w), 827 (s), 763 (m), 734 (m), 699 (s), 557 (s). ^1H NMR (400 MHz, $CDCl_3$), δ (ppm): 9.23 (s, 1 H), 8.61-8.42 (m, 3 H), 8.12 (m, 4 H), 7.86 (m, 4 H), 7.56-7.32(m, 24 H), 7.07 (m, 2 H), 6.75 (m, 1 H), 6.50 (m, 1 H). 3.41 (s, 3 H). ^{13}C NMR (101 MHz, $CDCl_3$), δ (ppm): 149.63, 148.55, 147.15, 140.11, 137.91, 136.57, 136.47, 136.13, 129.84, 129.67, 129.43, 129.33, 129.22, 129.17, 129.02, 128.99, 128.94, 128.65, 128.53, 128.46, 127.85, 126.44, 125.85, 125.62, 124.08, 123.57, 31.85. ^{19}F {^1H} NMR (377 MHz, $CDCl_3$), δ (ppm): -72.16 (d, 716.3 Hz). ^{31}P{^1H} NMR (162 MHz, $CDCl_3$), δ(ppm): -144.5 (hept., J=712.8 Hz). HRMS: $[M\text{-}PF_6]^+$ m/z 973.2599(experimental), 973.2578 (calculated). **RuNHC-2**, Yield: 90%, black solid. M.p: 258 ºC. IR (cm^{-1}): 1718 (w), 1479 (w), 1382 (m), 1317 (s), 1253 (w), 1202 (w), 1156 (w), 1109 (m), 1063 (m), 829 (s), 759 (m), 736 (m), 699 (s), 561 (s). ^1H NMR (400 MHz, DMSO-d_6), δ (ppm): 8.76 (d, J=5.6 Hz, 1 H), 8.47 (d, J=5.2 Hz, 1 H), 8.36 (d, J=7.2 Hz, 1 H), 8.30 (d, J=6 Hz, 1 H), 8.18 (m, 5 H), 8.01 (d, J=5.2 Hz, 1 H), 7.86-7.60 (m, 24 H), 7.45-7.18 (m, 4 H), 6.46 (d, J=1.6 Hz, 1 H), 3.29 (s, 3 H). ^{13}C NMR (101 MHz, DMSO-d_6), δ (ppm): 210.43, 176.59, 154.61, 153.80, 153.02, 149.58, 148.51, 148.36, 147.42, 146.65, 146.55, 146.35, 146.17, 145.99, 144.81, 136.76, 135.99, 135.91, 135.80, 131.82, 130.88, 129.87, 129.84, 129.79, 129.72, 129.33, 129.17, 129.07, 128.99, 127.95, 127.84, 127.64, 127.19, 126.59, 126.13, 126.05, 125.86, 125.69, 125.47, 125.28, 123.58, 122.99, 122.58, 121.50, 111.48, 110.64, 110.03, 108.51, 32.23. ^{19}F {^1H} NMR (377 MHz, DMSO-d_6),

δ (ppm): -60.05 (s), -69.19 (d, J=712.5 Hz). $^{31}P\{^{1}H\}$ NMR (162 MHz, DMSO-d_6), δ(ppm): -144.2 (hept., J=712.8 Hz). HRMS: $[M\text{-}PF_6]^+$ m/z 1041.2455(experimental), 1041.2467 (calculated). **RuNHC-3**, Yield: 92%, black solid. M.p: 274 °C. IR (cm^{-1}): 1727 (w), 1563 (w), 1430 (w), 1324 (w), 1249 (w), 1200 (w), 1080 (w), 1033 (w), 829 (s), 767 (m), 736 (m), 700 (s), 549 (s). ^{1}H NMR (400 MHz, DMSO-d_6), δ (ppm): 8.72 (d, J=5.6 Hz, 1 H), 8.47 (dd, J=12, 5.2 Hz, 2 H), 8.26 (d, J=8 Hz, 1 H), 8.17 (d, J=4.8 Hz, 4 H), 7.94 (m, 2 H), 7.83 (d, J=5.6 Hz, 1 H), 7.78 (d, J=5.6 Hz, 2 H), 7.70-7.55 (m, 21 H), 7.49 (d, J=8 Hz, 1 H), 7.32 (m, 3 H), 6.49 (dd, J=8.4, 2.8 Hz, 1 H), 3.45 (s, 3 H), 3.25 (s, 3 H). ^{13}C NMR (101 MHz, DMSO-d_6), δ (ppm): 208.20, 176.63, 154.97, 154.19, 153.72, 149.61, 148.49, 148.31, 147.62, 146.44, 146.32, 146.23, 146.12, 145.59, 144.20, 143.33, 136.43, 136.08, 136.04, 135.98, 135.89, 131.57, 129.93, 129.86, 129.83, 129.75, 129.29, 129.22, 129.11, 129.06, 128.99, 127.85, 127.83, 127.59, 127.06, 126.12, 126.03, 125.90, 125.78, 125.63, 125.41, 125.25, 122.61, 122.30, 121.86, 112.16, 110.08, 109.69, 104.34, 54.07, 32.02. $^{19}F\ \{^{1}H\}$ NMR (377 MHz, DMSO-d_6), δ (ppm): -69.19 (d, J=712.5). $^{31}P\{^{1}H\}$ NMR (162 MHz, DMSO-d_6), δ(ppm): -144.2 (hept., J=712.8 Hz). HRMS: $[M\text{-}PF_6]^+$ m/z 1003.2676(experimental), 1003.2698(calculated).

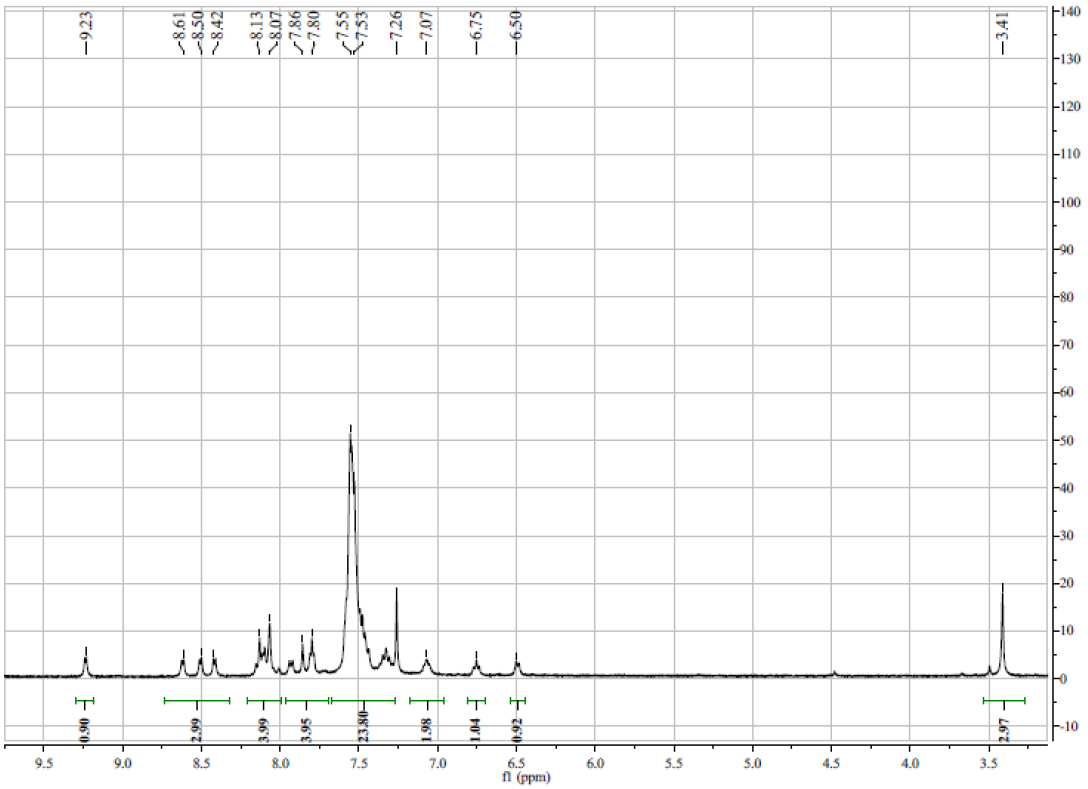

Fig. S1. ^{1}H NMR spectra of RuNHC-1 in $CDCl_3$.

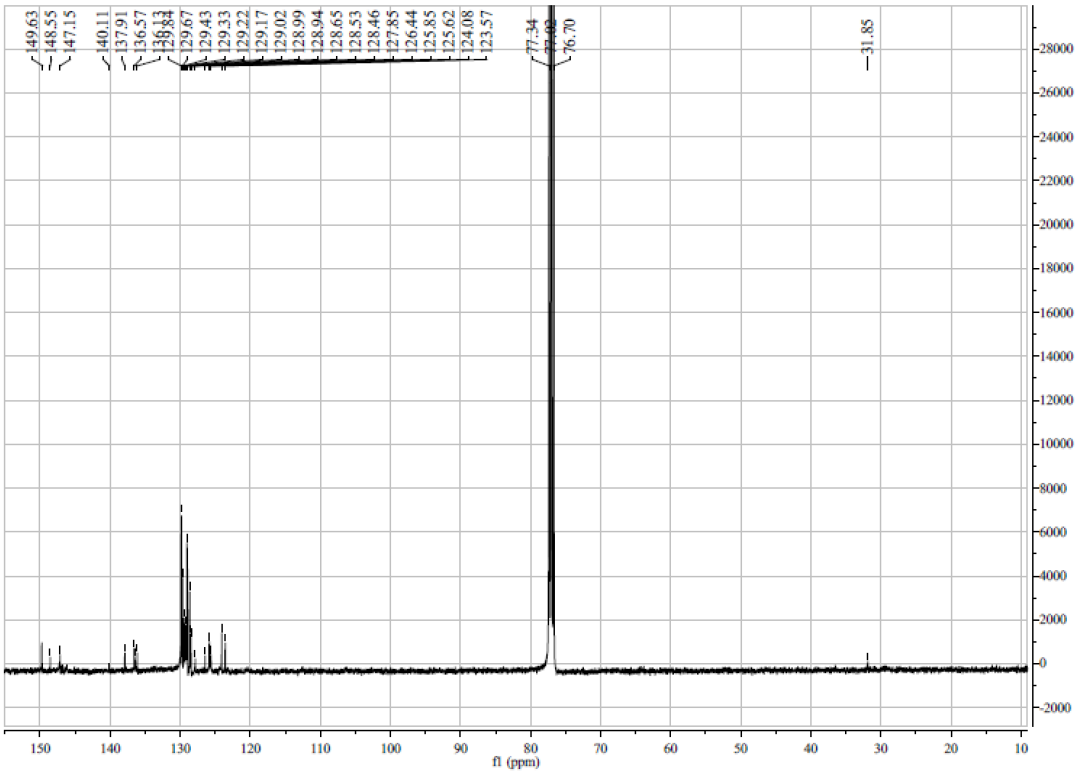

Fig. S2. ^{13}C NMR spectra of RuNHC-1 in $CDCl_3$.

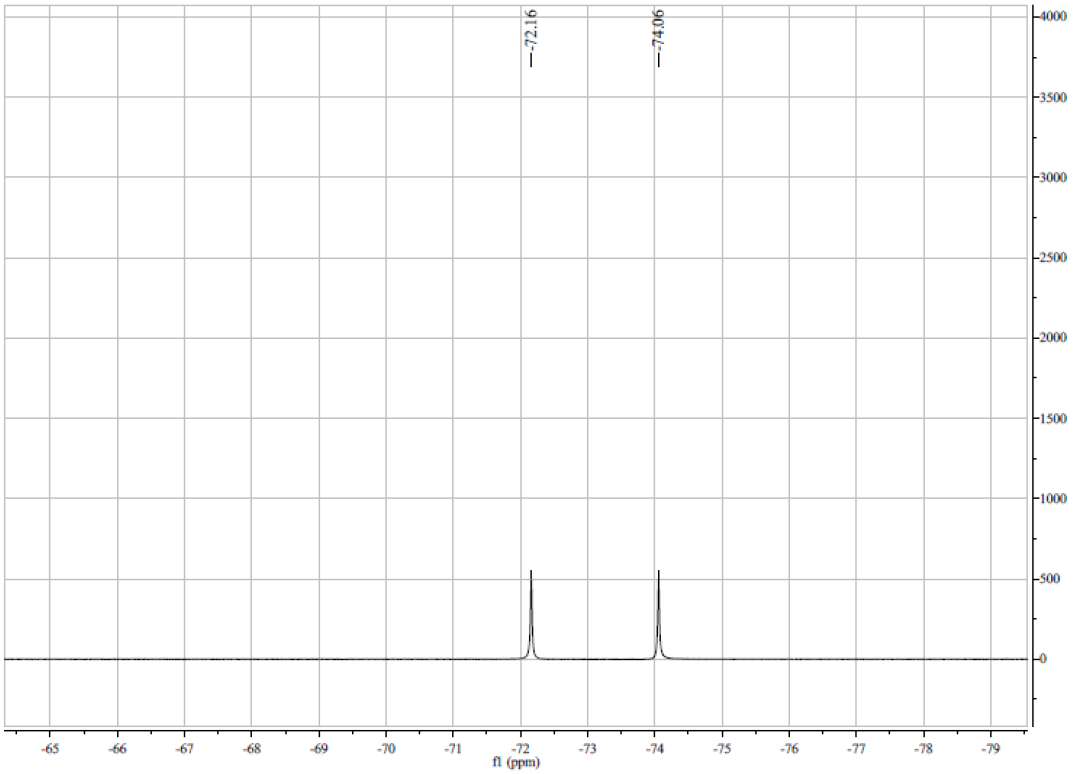

Fig. S3. ^{19}F NMR spectra of RuNHC-1 in $CDCl_3$.

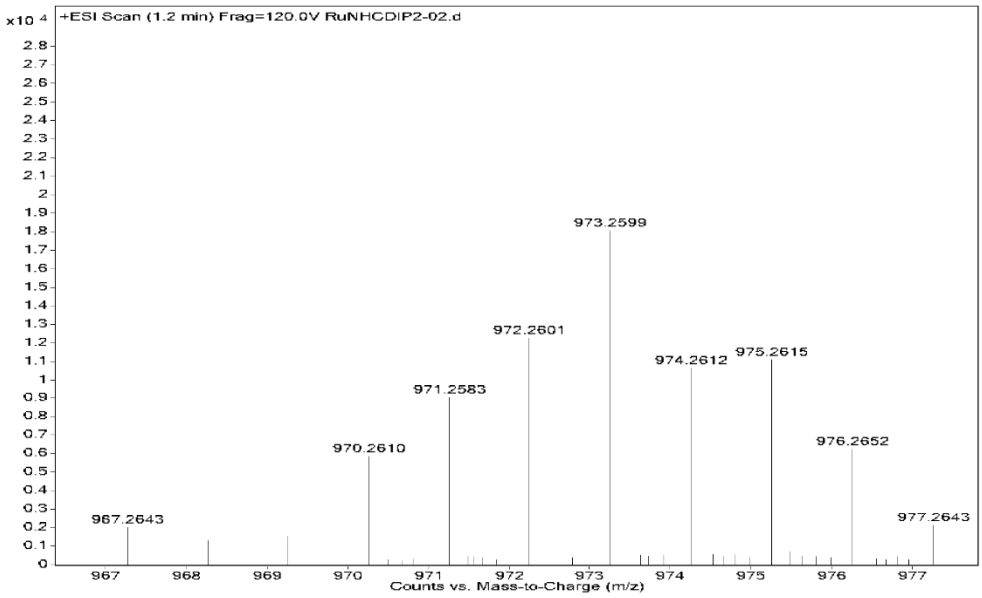

Fig. S4. HRMS of RuNHC-1.

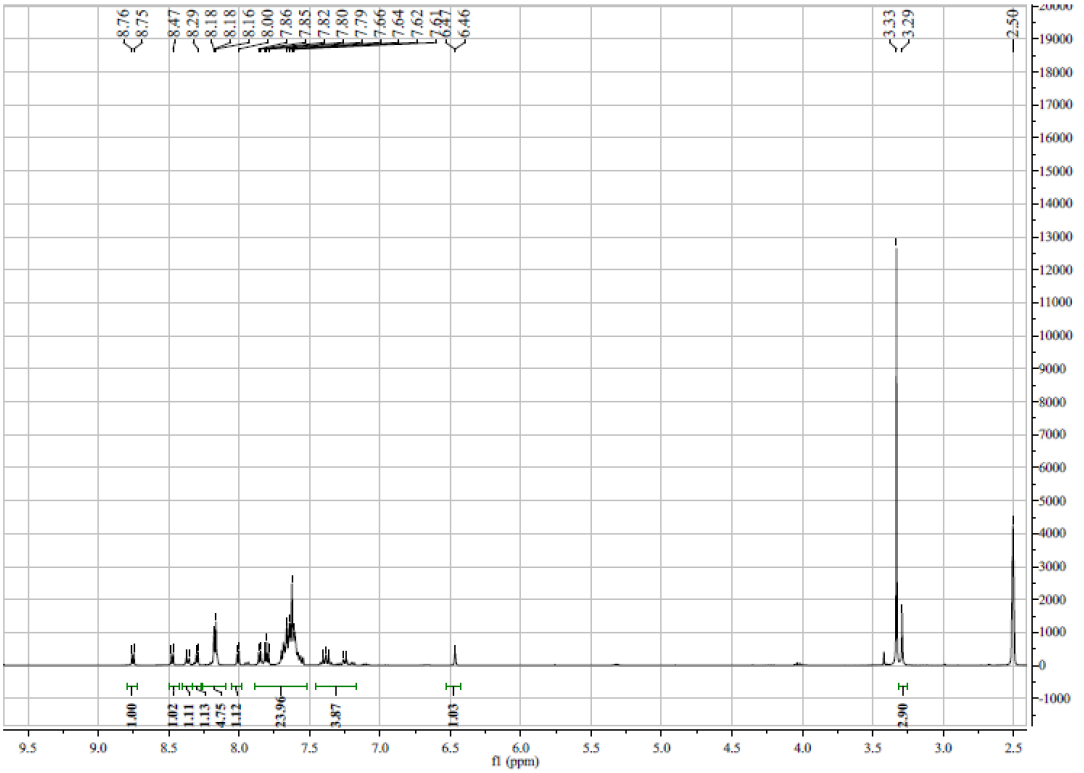

Fig. S5. ^{1}H NMR spectra of RuNHC-2 in DMSO-d_6.

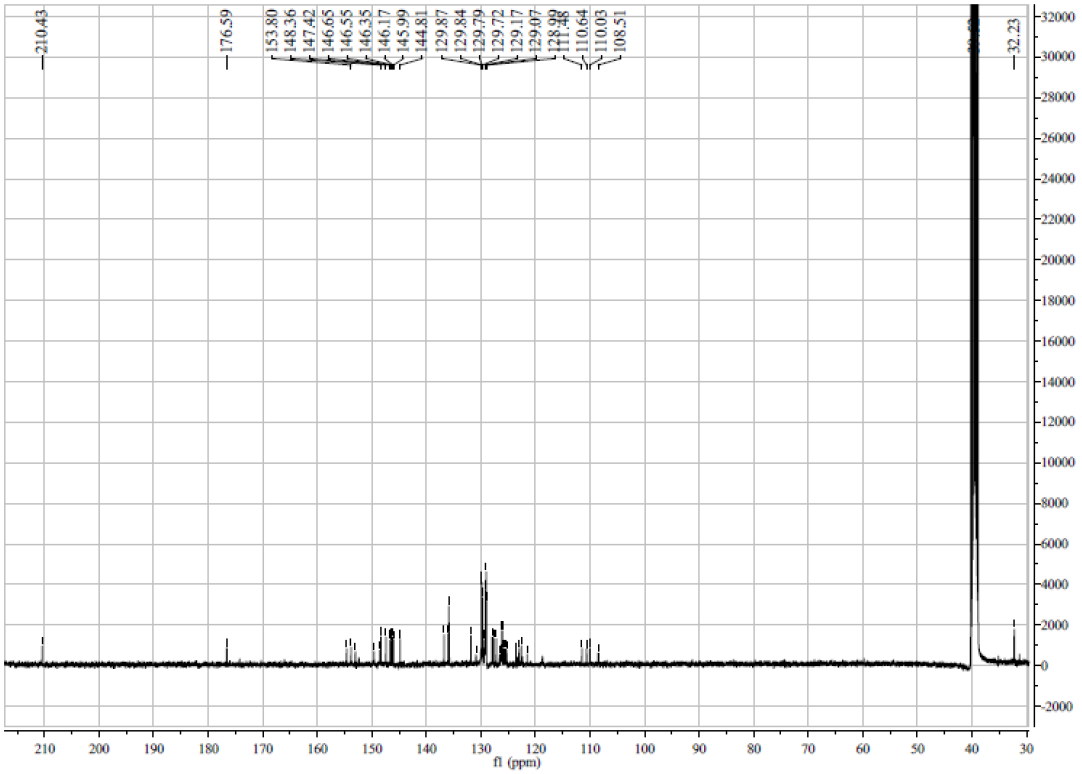

Fig. S6. ^{13}C NMR spectra of RuNHC-2 in DMSO-d_6.

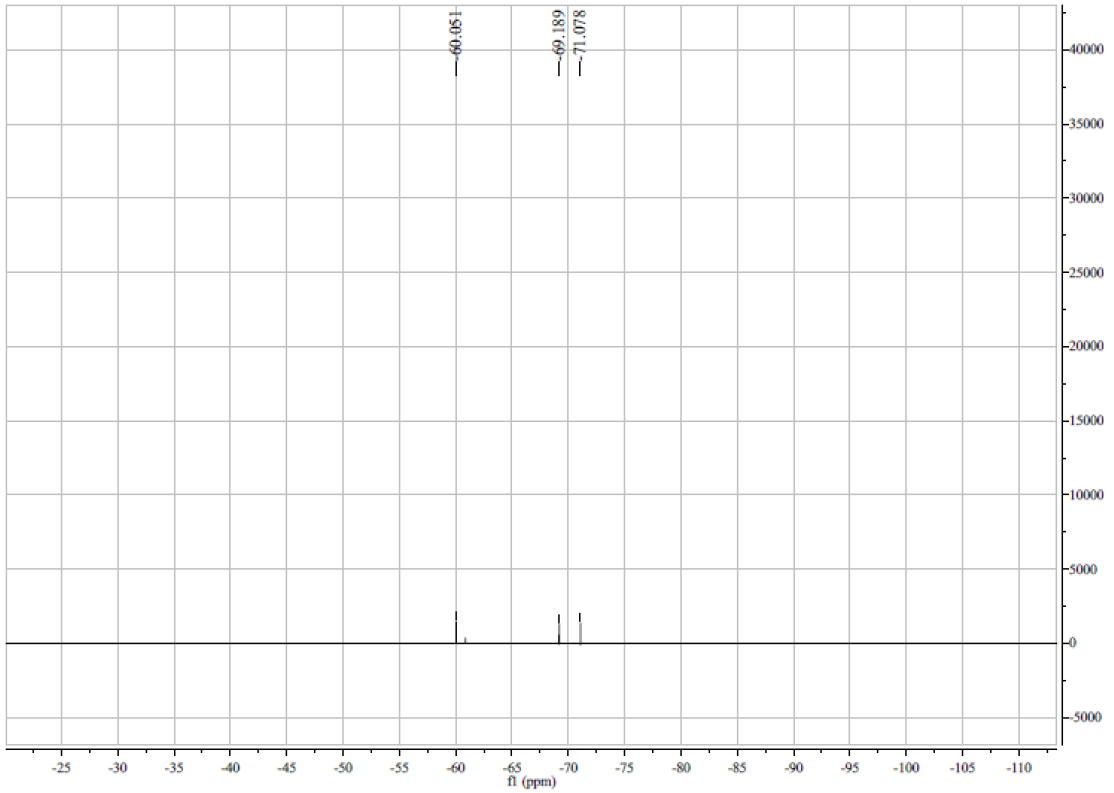

Fig. S7. ^{19}F NMR spectra of RuNHC-2 in DMSO-d_6.

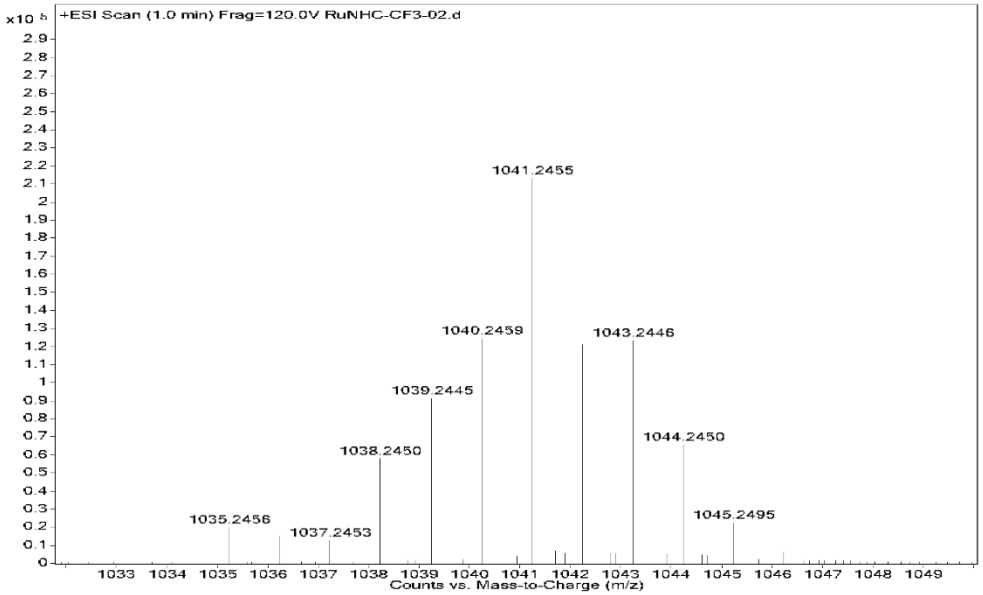

Fig. S8. HRMS of RuNHC-2.

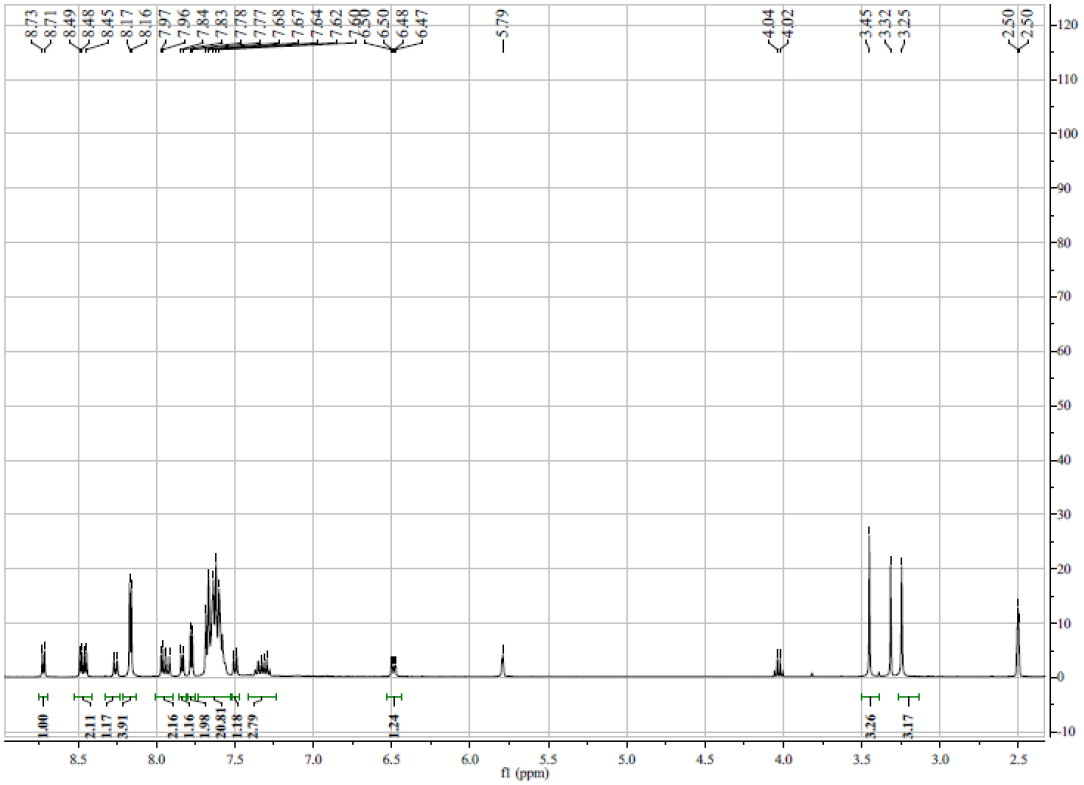

Fig. S9. ^{1}H NMR spectra of RuNHC-3 in DMSO-d_6.

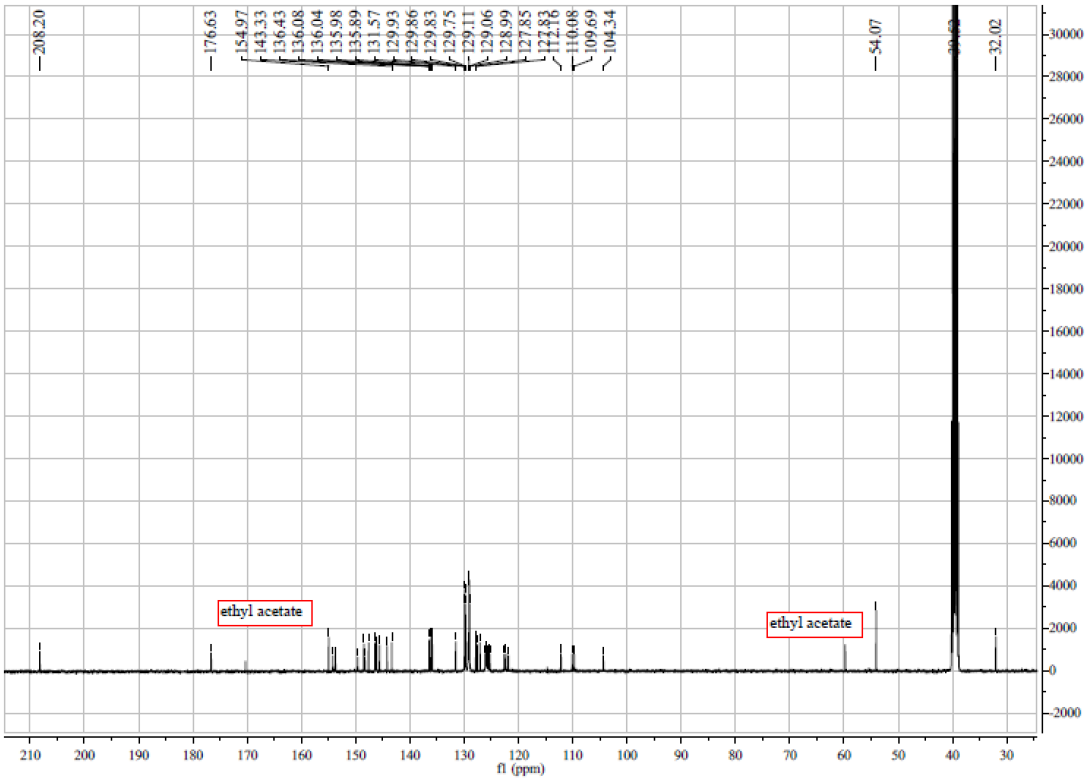

Fig. S10. ^{13}C NMR spectra of RuNHC-3 in DMSO-d_6.

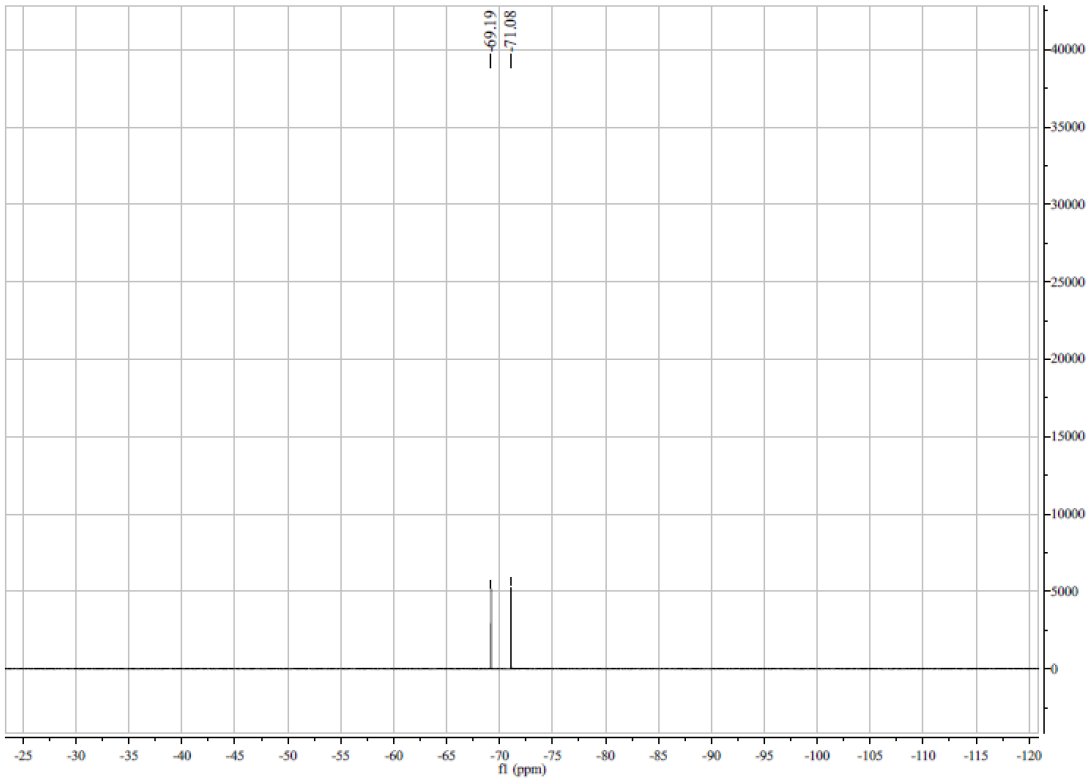

Fig. S11. ^{19}F NMR spectra of RuNHC-3 in DMSO-d_6.

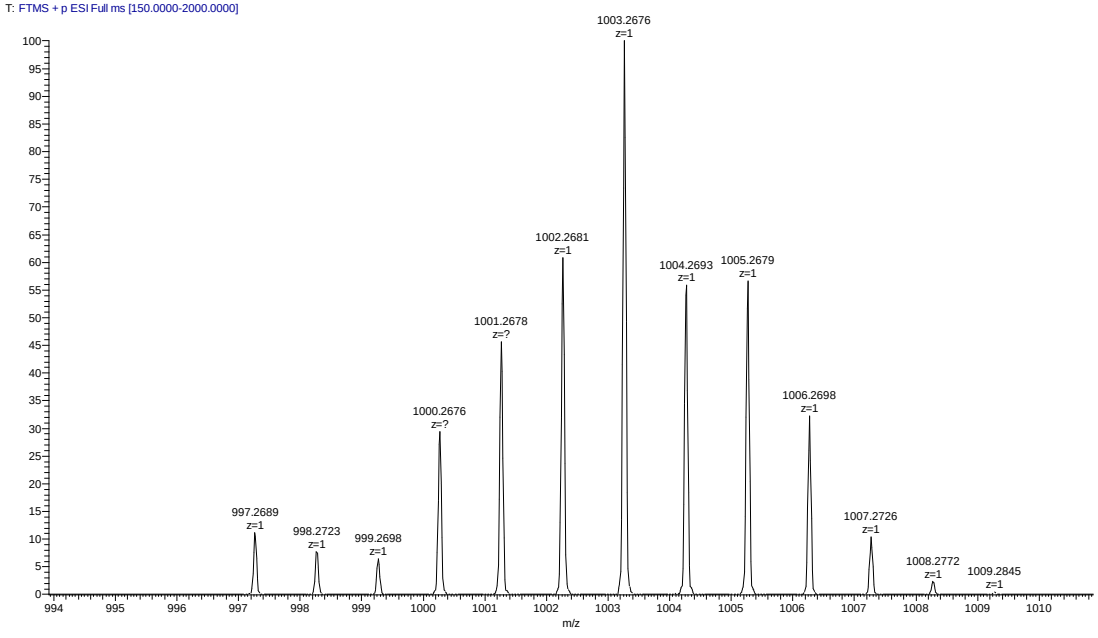

Fig. S12. HRMS of RuNHC-3.

2. Photophysical data

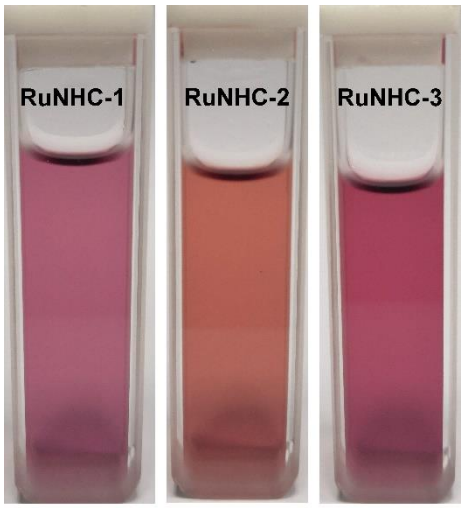

Fig. S13. The photographs of 40 μM RuNHC complexes in acetonitrile solutions.

Table S1. Absorption and photoluminescent data of RuNHC complexes in acetonitrile solution at room temperature.

Complexes	Absorption	Photoluminescence (PL)	
	λ_{max}/nm [εx10^{-4} M^{-1} cm^{-1}]	λ_{max}/nm	Φ_{PL}[a]
RuNHC-1	277[10.36];316[3.60]; 479[1.86]; 528[1.61]	823	0.13%
RuNHC-2	276[9.06];316[3.08]; 470[1.80]; 527[1.38]	781; 616	0.46%
RuNHC-3	278[11.08];317[3.99]; 479[2.21]; 532[1.94]	816	0.11%

a. referred to $Ru(bpy)_3^{2+}$ (Φ_{PL}=6.2%) in acetonitrile, N_2-saturated condition.

3. CV of RuNHC complexes

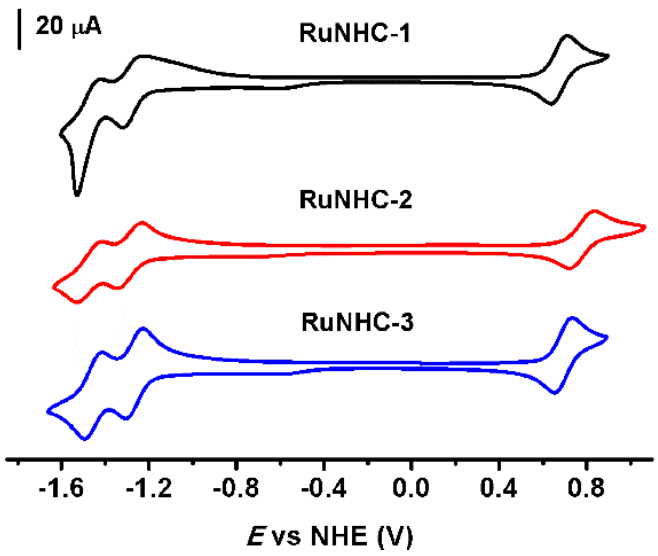

Fig. S14. CV spectra of 1 mM RuNHC complexes containing 0.1 M $TBAPF_6$ in anhydrous acetonitrile solution (saturated with argon). Scan rate: 100 mV/s; The working electrode is glassy carbon (GC) and the diameter of GC is 3 mm.

4. Theoretical calculations

In order to further investigate the inherent natures of photophysical properties, density functional theory (DFT) and time dependent density functional theory (TD-DFT) were employed to calculate the ground and excited states of these novel ruthenium(II) complexes. In order to simplify the chemical structures for calculation, the counter anion of hexafluorophosphate in these complexes has been omitted in the geometry optimization.

First, the ground states of these complexes have been optimized by DFT calculations with incorporating acetonitrile as solvent model. Fig. S15 presented the contour plots of HOMO and LUMO energy levels of ruthenium(II)-based NHC complexes in this work, including the corresponding electronic distributions on the frontier orbitals. The electrons in the HOMO orbital are mainly distributed on metal center and phenyl part of C^C* ligands, while two DIP ligands contributed the electrons on the LUMO orbital. Compared with very slight influences on LUMO energy level, the substituents has distinct effect on the HOMO energy level of these ruthenium(II)

complexes. Compared with RuNHC-1, RuNHC-2 with electron-withdrawing substituent of -CF_3 have lower HOMO energy level, meanwhile, RuNHC-3 with electron-donating substituent of -OMe have higher HOMO energy level, which demonstrated the HOMO of ruthenium(II) complexes could be stabilized by -CF_3 on the phenyl part of the C^C* ligands. In all, though theoretical calculation results are inconsistent with the PL experimental results between RuNHC-1 and RuNHC-3, RuNHC-2 with largest energy gaps from theoretical calculation displayed PL with shortest wavelength among them.

Based on the optimized ground states, TD-DFT calculations were further employed to investigate excited states (S_1 and T_1) of these ruthenium(II) NHC complexes. The crucial calculation results of the excited states have been presented in Table S2. As the representatives of excited states closely with photophysical properties, the electronic transitions of S_1 and T_1 for these new ruthenium(II) complexes are a little complicated according to the assignments in Table S2. After analyzing the electronic distributions on frontier orbitals involving the transitions of S_1 and T_1, we can reasonably conclude that the majority of emission natures should be ascribed to the mixtures of metal to ligand (DIP) charge transfer (MLCT) and ligand (C^C*) to ligand (DIP) charge transfer (LLCT). The shoulder peaks at 610 nm observed in PL spectra maybe are related with complicated compositions of excited states of these RuNHC complexes.

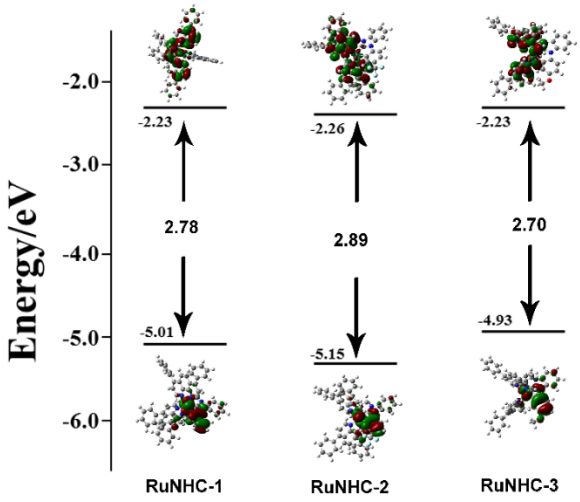

Fig. S15. Contour plots of HOMO and LUMO of RuNHC complexes in this work.

Table S2. Calculated transition wavelength, oscillator strength (f) and molecular orbitals involved in the lowest-energy transition of RuNHC complexes in this work.

Complexes	States	λ_{max}/nm	f	Assignments
RuNHC-1	T_1	671.00	0.0000	HOMO→LUMO (39.29%)
				HOMO→LUMO+1 (+17.62%)
				HOMO→LUMO+2 (49.99%)
	S_1	606.12	0.0214	HOMO→LUMO (63.10%)
				HOMO→LUMO+1 (18.07%)
				HOMO→LUMO+2 (+21.61%)
RuNHC-2	T_1	638.79	0.0000	HOMO→LUMO (+38.78%)
				HOMO→LUMO+1 (29.58%)
				HOMO→LUMO+2 (45.70%)
	S_1	578.44	0.0193	HOMO→LUMO (61.15%)
				HOMO→LUMO+1 (25.87%)
				HOMO→LUMO+2 (19.73%)
RuNHC-3	T_1	677.32	0.0000	HOMO→LUMO (41.69%)
				HOMO→LUMO+1 (+20.96%)
				HOMO→LUMO+2 (45.26%)
	S_1	614.55	0.0388	HOMO→LUMO (65.32%)
				HOMO→LUMO+1 (13.97%)
				HOMO→LUMO+2 (+16.18%)

5. Optimization of co-reactants

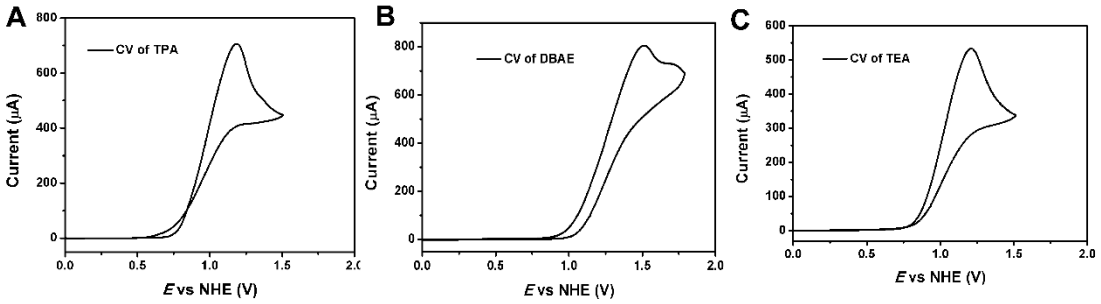

Fig. S16. CV of 40 mM co-reactants (A: TPA; B: DBAE; C: TEA) containing 0.1 M $TBAPF_6$ in anhydrous acetonitrile solution (saturated with argon atmosphere). Scan rate: 0.1 V/s; The working electrode is glassy carbon and the diameter is 3 mm.

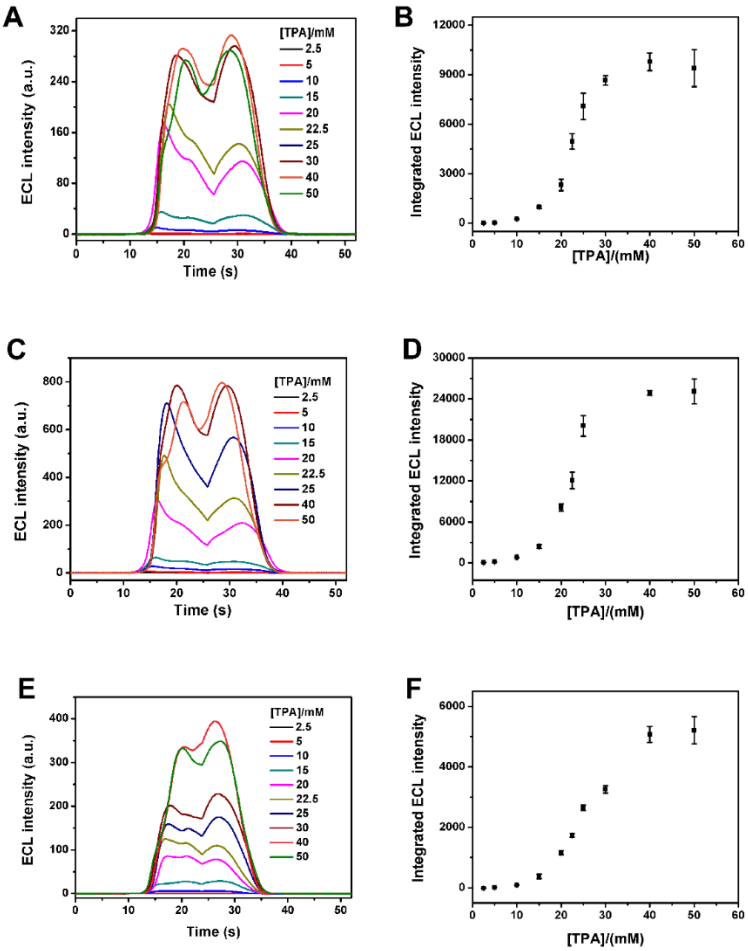

Fig. S17. The ECL intensity (A, C, E) and corresponding integrated ECL intensity data (B, D, F) of 0.1 mM ruthenium(II) NHC complexes (A, C, E are referred to RuNHC-1, RuNHC-2 and RuNHC-3, respectively) with different concentrations of TPA under potential scanning experiments in anhydrous acetonitrile solutions. scan rate is 50 mV/s, supporting electrolyte is 0.1 M TBAPF.

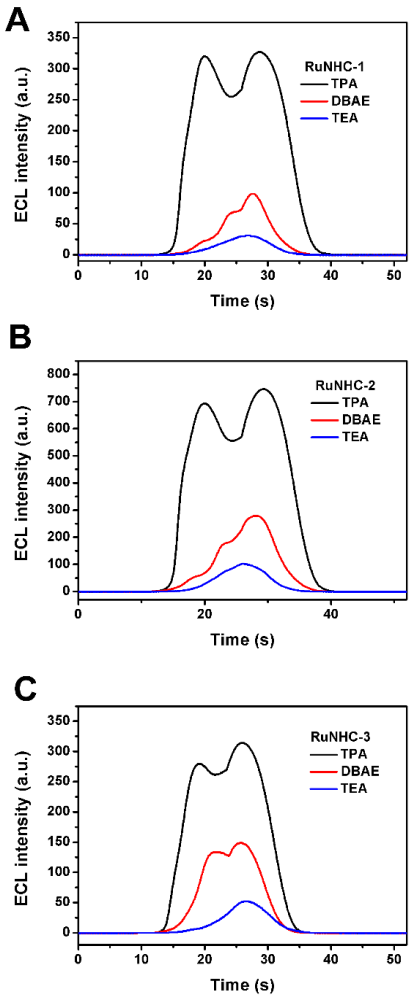

Fig. S18. The ECL intensity comparison studies of ruthenium(II) NHC complexes (A is RuNHC-1, B is RuNHC-2 and C is RuNHC-3) with different oxidative-reduction co-reactants (black line, red line and blue lines are TPA, DBAE and TEA, respectively) in potential scanning conditions. The concentrations of RuNHC complex and co-reactants are 0.1 mM and 40 mM, respectively. The supporting electrolyte is 0.1 M $TBAPF_6$, scan rate is 50 mV.

As one kind of novel ECL luminophores, the relationships between the concentrations of TPA and the ECL intensity of RuNHC complexes have been thoroughly revealed in this work. First, ECL experiments based on positive potential scanning mode has been carried out in this work. In order to comparing the absolute ECL intensity obviously, Fig. S17 shows the ECL curves as a function of time with various concentration of TPA (Fig. S17A, S17C&S17E). According to Fig. S17, the ECL intensities of RuNHC complexes in this work are increasing along with the addition of TPA and the ECL intensity achieved the peak values when the ratios of [TPA]/[RuNHC] is 400. Taking into account other amines also as excellent “oxidative-

reduction" co-reactants reported in the former literatures[3, 4], 2-(dibutylamino)ethanol (DBAE), triethylamine (TEA) have also been employed as the co-reactants to generate ECL of these novel ruthenium(II) NHC complexes in this work. The comparison experimental results including TPA, DBAE and TEA have been listed in Fig. S18. It's found that TPA outperforms DBAE and TEA as the co-reactants of these novel ruthenium(II) complexes under positive potential scanning ECL mode.

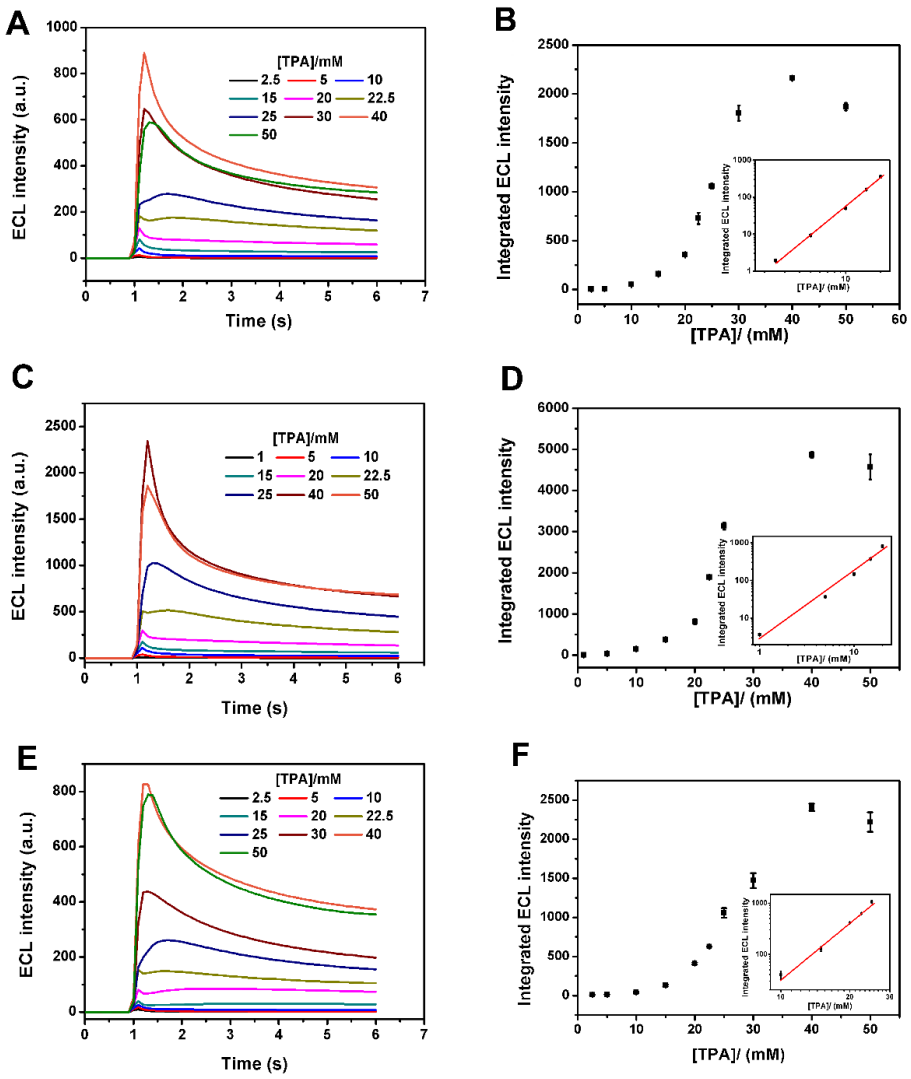

Fig. S19. The ECL intensity (A, C, E) and corresponding integrated ECL intensity data (B, D, F) of 0.1 mM RuNHC complexes (A, C, E are referred to RuNHC-1, RuNHC-2 and RuNHC-3, respectively) with different concentrations of TPA under potential stepping experiments (the potential was set at 1.6 V vs NHE) in anhydrous acetonitrile solutions. Scan rate is 50 mV/s, supporting electrolyte is 0.1 M TBAPF. The inset is the linear relationship between integrated ECL intensity and the concentration of TPA.

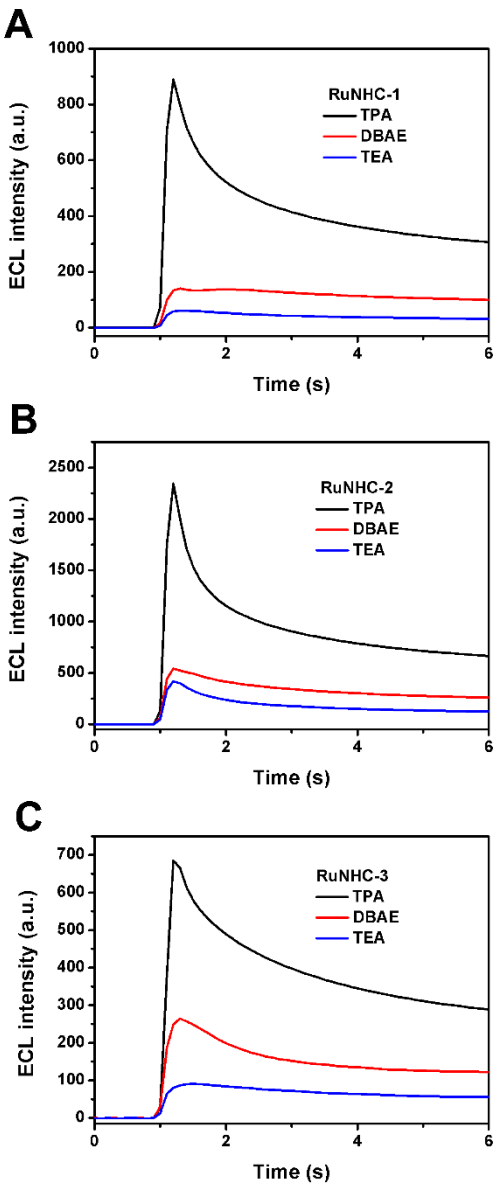

Fig. S20. The ECL comparison studies of ruthenium(II) NHC complexes (A is RuNHC-1, B is RuNHC-2 and C is RuNHC-3) with different oxidative-reduction co-reactants (black line, red line and blue lines are TPA, DBAE and TEA, respectively) in potential stepping conditions. The potential was set at *ca.* 400 mV past over the peak oxidation potential of corresponding co-reactant.

Fig. S19 shows the ECL intensity of RuNHC complexes as a function of time with various concentration of TPA under the potential stepping mode. Obviously, all these RuNHC complexes in acetonitrile solution with TPA as co-reactant have also displayed ECL signals when applied the potential (1.6 V *vs* NHE) on GC electrode. Furthermore, the ECL intensities of RuNHC complexes are going up along with the increase of the concentration of TPA. The accurate relationship between the concentration of TPA and ECL intensity of RuNHC complexes under potential stepping mode have also been

plotted in Fig. S19 accordingly (presented in Fig. S19B, S19D&S19E). The inset pictures in Fig. S19B, S19D&S19E showed the double logarithms plots between ECL intensity and the concentration of TPA. It's found that the ECL intensities have a very good linear relationship (R^2>0.99) with the concentration of TPA in some concentration ranges (RuNHC-1: 2.5~20 mM, fitting equation is $y=-0.86+2.62x$; RuNHC-2: 1~20 mM, fitting equation is $y=0.50+1.76x$; RuNHC-3: 20~25 mM, fitting equation is $y=-2.25+3.74x$). The revealed mathematic equations would be very helpful for both ECL optimization of new luminophores and potential analytical applications. The further comparison ECL studies of various co-reactant have also been carried out. Just as shown in Fig. S20, TPA, DBAE and TEA have all been employed as co-reactant for RuNHC complexes in this work to generate ECL under potential stepping mode. The experimental results demonstrate that TPA is still the best co-reactant among them in the potential stepping ECL studies for all these three RuNHC complexes.

6. The potential stepping ECL of RuNHC complexes with BPO as co-reactant.

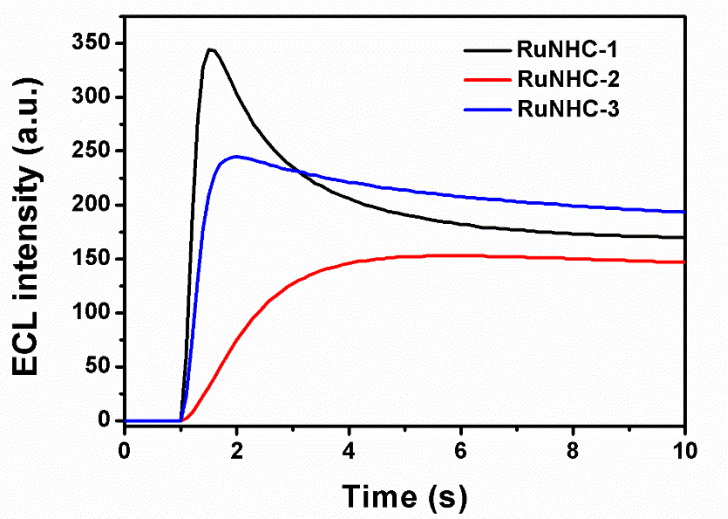

Fig. S21. The potential stepping ECL performance of 0.1 mM RuNHC complexes in acetonitrile solutions containing 0.1 M $TBAPF_6$ and 40 mM BPO. Potential was set 0 V for 1 s and -1.85 V (vs NHE) for 10 s.

7. The annihilation ECL of RuNHC complexes

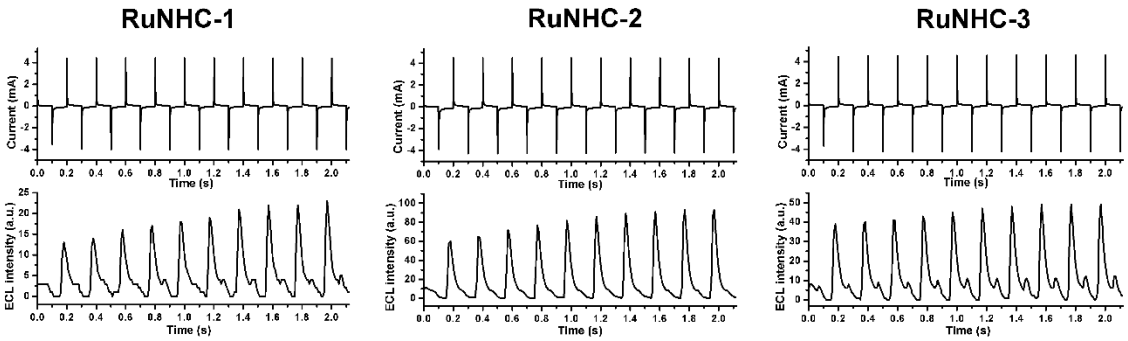

Fig. S22. The annihilation ECL of 0.1 mM RuNHC complexes in argon-saturated acetonitrile solution with 0.1 M TBAPF6. (pulsing width is 0.1 s, the acquisition rate of photocurrent is 100 T/s, high potential: 1.0 V vs NHE, low potential: -1.7 V vs NHE).

8. ECL performance of RuNHC in aqueous ProCell solution.

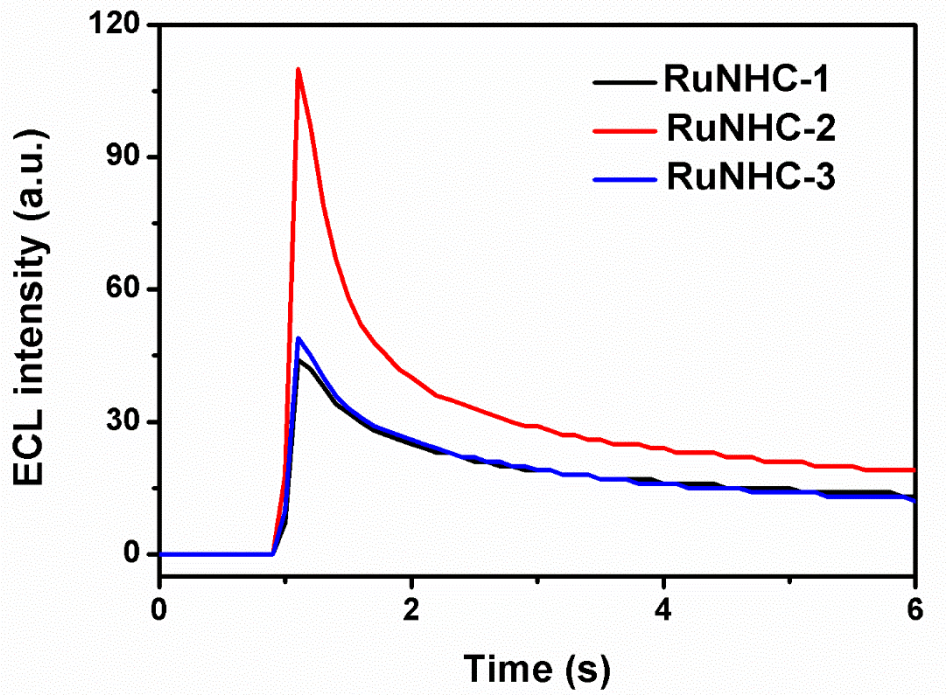

Fig. S23. The ECL performance of 0.1 mM RuNHC complexes in aqueous ProCell solution under potential stepping mode. Potential as set at 1.4 V vs Ag/AgCl.

References

1. V. V. Pavlishchuk and A. W. Addison, *Inorg. Chim. Acta*, 2000, **298**, 97-102.
2. M. Bandini, M. Bianchi, G. Valenti, F. Piccinelli, F. Paolucci, M. Monari, A. Umani-Ronchi and M. Marcaccio, *Inorg. Chem.*, 2010, **49**, 1439-1448.
3. X. Liu, L. Shi, W. Niu, H. Li and G. Xu, *Angew. Chem. Int. Ed.*, 2007, **46**, 421-424.
4. M. Zhao, A.-Y. Chen, D. Huang, Y.-Q. Chai, Y. Zhuo and R. Yuan, *Anal. Chem.*, 2017, **89**, 8335-8342.